In-situ STM study of phosphate adsorption on Cu(111), Au(111) and Cu/Au(111) electrodes

Schlaup, Christian; Horch, Sebastian

Published in:
Surface Science

Link to article, DOI:
10.1016/j.susc.2012.09.011

Publication date:
2013

In-situ STM study of phosphate adsorption on Cu(1 1 1), Au(1 1 1) and Cu/Au(1 1 1) electrodes

Christian Schlaup[a,*], Sebastian Horch[a]

[a] *Technical University of Denmark, Department of Physics, DK–2800 Kongens Lyngby, Denmark*

Abstract

The interaction of Cu(1 1 1), Au(1 1 1) and Cu-covered Au(1 1 1) electrodes with a neutral phosphate buffer solution has been studied by means of cyclic voltammetry (CV) and in situ electrochemical scanning tunneling microscopy (EC-STM). Under low potential conditions, both the Cu(1 1 1) and the Au(1 1 1) surface appear apparently adsorbate free, indicated by the presence of a (4×4) structure and the herringbone surface reconstruction, respectively. Upon potential increase, phosphate anions adsorb on both surfaces and for Cu(1 1 1) the formation of a $(\sqrt{3}\times\sqrt{3})R30°$ structure is found, whereas on Au(1 1 1) a "$(\sqrt{3}\times\sqrt{7})$" structure is formed. For a Cu-*sub*monolayer on Au(1 1 1), coadsorption of phosphate anions leads to the formation of a (2×2) vacancy structure within an assumed pseudomorphic structure of the Cu-submonolayer with the phosphate anions occupying the vacancies. When desorbing the phosphate anions at low potentials, the Cu-submonolayer first becomes mobile and eventually undergoes an irreversible transition to a coalescent *nonpseudomorphic* structure.

Keywords: Scanning tunneling microscopy, Electrochemical phenomena, Catalysis, Copper, Phosphate, Carbon dioxide

1. Introduction

The adsorption of anions at metal electrode surfaces is a major topic in the field of interfacial electrochemistry and has been extensively studied over the past utilizing various methods [1]. Thereby their influence on the morphology and structure of the basal planes of single crystaline noble metal electrodes, such as Cu, Au and Pt, was of particular interest. But also their influence on the electrochemical metal deposition, in particular on ultrathin metal (sub-) monolayers formed by underpotential deposition (upd) was studied in great detail [2]. However, most of these studies focus on halide anions or sulfate, as a representative of molecular oxo-anions, whereas other anionic species have drawn much less attention. In particular the interaction of copper surfaces with phosphate anions has not been studied extensively, yet.

This is quite surprising, as this particular system not only is interesting in terms of anion adsorption, but also is an ideal model system for studying the

*Corresponding author

Email address: cgsc@fysik.dtu.dk (Christian Schlaup)

electrochemical reduction of CO_2 to hydrocarbons, e.g. methane, which would allow to store electrical energy in chemical bond and thus establish a sustainable carbon dioxide cycle [3] for energy utilization. For this purpose, copper electrodes are known experimentally [4, 5, 6] and from theoretical studies [7, 8] to exhibit the highest activity of all pure metal electrodes, however they are still very inefficient, i.e. have a huge overpotential, to drive this reaction. As the origin of the overpotential, the relative binding strength of some reaction intermediates with the copper surface has been identified, which needs to be changed in order to achieve a higher catalytic activity [7, 8]. A possibility to modify the binding energies of adsorbate is to introduce strain into the surface of the substrate [9], e.g. by deposition of a pseudomorphic Cu-(sub)monolayer on a Au(1 1 1) surface which has a 12.5% greater lattice constant than bulk Cu(1 1 1). However, the conditions under which such an ultrathin metal film remains in a pseudomorphic structure and does not collapse to a more compact structure need to be carefully determined.

In the present study we characterize the surface structures of Cu(1 1 1), Au(1 1 1) and Cu-covered Au(1 1 1) electrodes in contact with a CO_2 free 0.05 M KH_2PO_4 + 0.05 M K_2HPO_4 phosphate buffer solution (pH = 6.8), which was chosen having the use of the present systems as model systems for CO_2 reduction in mind [10]. It behaves inert for CO_2 reduction, in contrast to e.g. a carbonate buffer solution. Furthermore it allows a precise pH adjustment, considering the bicarbonate/carbonate equilibrium of solved CO_2, and the hydrogen evolution reaction (HER) which may compete with CO_2 reduction.

2. Experimental

All experiments were carried out in a custom built EC-STM setup which combines a standard three-electrode electrochemical cell with a Besocke-type scanning tunneling microscope [11]. The electrochemical cell is equipped with two Platinum wires that act as counter- and pseudo reference electrode, respectively. The potential of the Pt/PtO pseudo-reference electrode for the different electrolytes was calibrated against a NHE electrode. In order to provide comparability, all potentials reported in the following are given with respect to the standard hydrogen electrode (SHE). The stability of the pseudo-reference electrode may be an issue in acidic solutions, as used for the Cu-deposition on the Au(1 1 1) electrode, and was carefully considered for each experiment. However, in the neutral and pH-buffered phosphate buffer solution it is much more stable, probably due to the formation of stable PtO layers, and even after several hours of experiments only small potential deviations of less than ±25 mV were observed. STM tips were etched electrochemically from a Pt/Ir (90/10) wire with 0.25 mm diameter and insulated with hot-glue (PEVAC). All STM images were recorded in constant current mode with a typical acquisition time of about 20 s for a high resolution image.

Commercially available Cu(1 1 1) and Au(1 1 1) single crystals (MaTecK, Jülich) have been prepared prior to each experiment using well-known procedures: the copper crystal was electropolished in 50 % H_3PO_4 at a voltage of 2 V against Platinum

and rinsed with deaerated MilliQ water, the gold crystal was flame-annealed in a butane/air flame at red heat and cooled down to room temperature in a high purity argon atmosphere. Both preparation methods yield clean and well defined surfaces for STM investigations. In order to avoid contaminations, the Cu(1 1 1) crystal was not exposed to a halide containing electrolyte which can be used to increase the mobility of step edges [12], therefore its average terrace width was significantly smaller than that of the flame annealed Au(1 1 1) single crystal.

Electrolyte solutions were prepared using Milli-Q water (18.2 MOhm cm, 2 ppb TOC), H_2SO_4, KH_2PO_4, K_2HPO_4 (all Suprapur, Merck) and $CuSO_4$ (p.A., Merck); before usage they have been deaerated with high purity Argon (99.9999%, 6.0). Even though the dominant anionic species in a 0.05 M KH_2PO_4 + 0.05 M K_2HPO_4 phosphate buffer solution (pH = 6.8), as used in the present study, is dihydrogenphosphate, in the following discussion the term *phosphate* is used for denoting any adsorbed anionic phosphate species, as, like for the discussion of (bi)sulfate adsorption, the exact chemical nature of the adsorbed phosphate species remains unclear.

All glassware was cleaned in Caroic's acid, followed by immerging it into 10 M KOH and extensive rinsing with Milli-Q water prior to usage.

3. Results

3.1. Cu(1 1 1) in PO_4 buffer solution

3.1.1. Cyclic voltammetry

A typical series of CV curves for a Cu(1 1 1) electrode in the phosphate buffer solution is presented in Fig. 1. A systematic variation of the scan range in anodic direction shows that the CV curve remains featureless up to a potential of −350 mV, except for the hydrogen evolution reaction (HER), which limits the scan range in cathodic direction (curve #1 in Fig. 1). Upon extension of the scan range in anodic direction, an additional broad anodic peak with a peak potential of −250 mV and three cathodic peaks close to the onset potential of the HER appear simultaneously (curve #2 and curve #3 in Fig. 1). By comparing both curves, it becomes clear that all three cathodic peaks appear even if the scan range is limited to −250 mV in anodic direction, i.e. before the broad anodic peak is fully passed during the anodic potential scan. Hence both features, the broad anodic peak and the three cathodic peaks, are related counter features. For both processes a charge exchange of 130 μC cm^{-2} is measured, corresponding to 0.5 ML of electrons with respect to the Cu(1 1 1) surface. At potentials above +100 mV an exponentially increasing anodic current and a pronounced cathodic peak during the back-scan are observed.

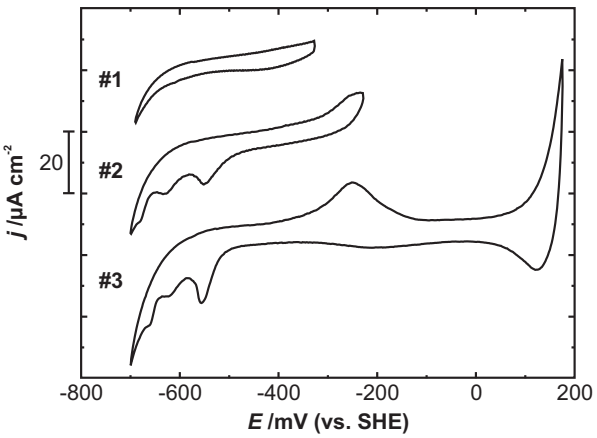

Figure 1: Series of CV curves for Cu(1 1 1) in a 0.05 M KH_2PO_4 + 0.05 M K_2HPO_4 solution, dE/dt = 10 mV s^{-1}.

A previous SERS study [13] revealed the adsorption of phosphate anions on copper electrodes starting at potentials of −0.6 V and 0.0 V for a $H_2PO_4^-$ (pH = 4.22) and a HPO_4^{2-} (pH= 9.31) solution, respectively. Assuming a linear relation between the adsorption potential and the pH of the solution, it appears reasonable to assign the anodic peak at −250 mV to the adsorption of phosphate anions from the neutral phosphate buffer solution used in the present study. Consequently, the three cathodic peaks appearing close to the onset of the HER correspond to the phosphate desorption. The peak pair above +100 mV can be assigned to the anodic copper dissolution and redeposition reactions, in agreement with previous results in neutral [14, 15] and weakly acidic [16] solutions as well as the Pourbaix diagram [17] whereupon Cu^{2+} cations are stable at potentials above +150 mV up to a pH of 7.3.

In addition, the Pourbaix diagram also predicts the formation of a Cu(I)-oxide phase at a potential of about 0 mV, which was also experimentally found for Cu(1 1 1) electrodes in contact with other neutral [14, 15] and weakly acidic [16] electrolytes. In these cases, the CV curves show an anodic peak close to the onset of the Cu dissolution reaction and a corresponding cathodic peak at approximately 300 mV more negative potentials. However, for the present system no evidence of the formation of a Cu(I)-oxide phase can be found. The *apparent* passivation against the formation of a Cu(I)-oxide phase can only be attributed to the presence of the phosphate adsorbate phase formed at −250 mV. Most likely, it is not just a simple anion adlayer, but a more complex mixed copper-oxo-phosphate phase. This is further supported by the pronounced kinetically hindering of its dissolution reaction, indicated by the large peak separation. Also the appearance of three distinguished phosphate desorption peaks indicates a rather complex desorption mechanism.

3.1.2. STM measurements

For the limited potential regime between the HER and the onset of phosphate adsorption, i.e. −700 and −350 mV, respectively, STM images show atomically flat terraces (Fig. 2a). The high step density of the Cu(1 1 1) surface is due to the fact that we intentionally avoid any thermal or electrochemical annealing during the sample preparation. However, the terrace width is still sufficient for STM investigations. The terraces are entirely covered with a hexagonal structure which can be described with a commensurate (4 × 4) unit cell (Fig. 2b).

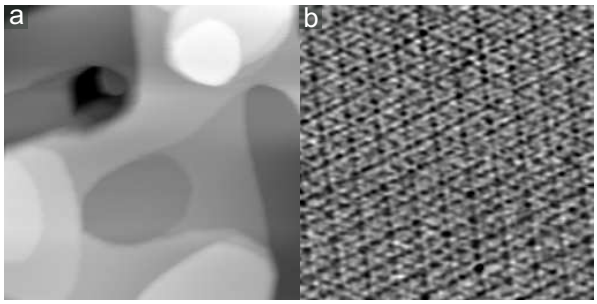

Figure 2: (a) Morphology, 114 × 114 nm^2, $E = -633$ mV, $U_B = 340$ mV, $I_T = 1$ nA; and (b) (4 × 4)-structure of the apparently adsorbate free Cu(1 1 1) surface at low potentials, 9.53 × 9.53 nm^2, $E = -594$ mV, $U_B = 11$ mV, $I_T = 20$ nA.

This structure is well known from other studies of Cu(1 1 1) electrodes in contact with other neutral, e.g. K_2SO_4 [15], and acidic, e.g. H_2SO_4 [18] and $HClO_4$ [19], electrolytes. Its unspecific appearance, which cannot be correlated with the presence of a

certain anion or cation species in the electrolyte, yields to its interpretation as an adsorbed water species, e.g. H_3O^+, OH^- or OH [19]. These studies also revealed a strong dependence of the apparent atomic features within the (4×4) unit cell on the bias voltage and tunnel current used for STM imaging, which has caused a misinterpretation of this phase as adsorbed organic molecules in the past [19]. Both, chemical nature and atomic structure of this (4×4) phase, are still unclear.

Recent EC-STM studies revealed a hydrogen-induced reconstruction of Cu(1 0 0) electrodes under low potential conditions [20, 21]. However, for the present system no morphological changes which would indicate a copper mass transport during either the formation or disappearance of the (4×4) phase were found and therefore an analog interpretation of the (4×4) phase as a reconstruction phase appears unlikely.

Independent from its actual chemical nature, the appearance of this structure indicates an only weak interaction of the Cu(1 1 1) surface with any phosphate anion species in the electrolyte. This is consistent with the results of the electrochemical characterization which revealed a featureless CV curve with this limited potential range (curve #1 in Fig. 1) and SERS results indicating an adsorbate free copper surface under low potential condition [13].

At only slightly higher potentials, i.e. the onset of the broad anodic peak in the CV curves, the surface topography changes and small patches appear on formerly atomically smooth terraces (Fig. 3a). High resolution STM images show that the (4×4) structure has disappeared on terraces and instead the (1×1) structure of the apparently adsorbate free Cu(1 1 1) surface is imaged, whereas the small patches exhibit a structure with hexagonal symmetry but significantly larger lattice constant (Fig. 3b). The possibility of imaging both structures in the same image allows a precise structure determination by internal calibration against the substrate, yielding in a commensurate $(\sqrt{3} \times \sqrt{3})R30^\circ$ unit cell for the structure of the patches. The boundaries of the patches are rather blurry, moreover, the $(\sqrt{3} \times \sqrt{3})R30^\circ$ structure appears in STM images superimposed with the (1×1) structure of the terraces (Fig. 3b). This indicates a continuous diffusion of the adsorbate along the boundaries of the patches and thus a rather weak bonding to the substrate.

According to the electrochemical characterization, we assign the $(\sqrt{3} \times \sqrt{3})R30^\circ$ structure to be formed by adsorbed phosphate anions. The local phosphate coverage within the patches can be directly deduced from their structure as 1/3 ML. For the areas in between different patches, the phosphate coverage cannot be determined from STM images, as they just show the (1×1) structure for these regions. However, the distinctive diffusion of phosphate anions along the boundaries of the patches strongly suggests that the terraces in-between the patches are covered with a mobile 2-dimensional gas-like phosphate anion adlayer. Since its condensation to the immobile patches does not occur preferentially at step edges (Fig. 3a), where it would be facilitated by additional Smoluchowski dipole moments, also point defects on terraces can be ruled out as nucleus for the patches. However, as this phase appears only in a very narrow potential range, it's most likely a kind of pre-

cursor for the formation of an amorphous copper-oxo-phosphate phase at slightly more anodic potentials, which will be discussed in the following section. Hence it appears reasonable that the immobile phosphate adlayer patches condensate at nuclei of the copper-oxo-phosphate formed during the initial stages of formation.

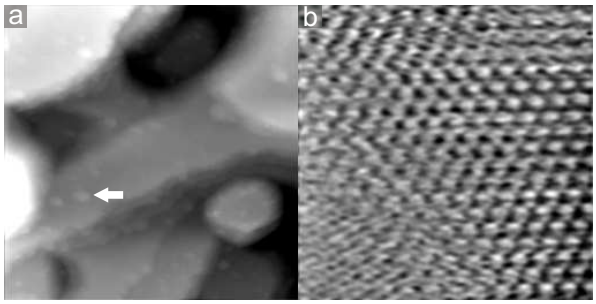

Figure 3: (a) Appearance of small patches (arrow) after potential increase, 114 × 114 nm^2, $E = -375$ mV, $U_B = 700$ mV, $I_T = 10$ nA; (b) high-resolution STM image of the $(\sqrt{3} \times \sqrt{3})R30°$-$PO_4$ adlayer, 5.72 × 5.72 nm^2, $E = -375$ mV, $U_B = 108$ mV, $I_T = 20$ nA.

A further potential increase does not lead to a stabilization of the phosphate adlayer and formation of larger patches, instead an amorphous phase with granular appearance is formed (Fig. 4a). Its grains exhibit a corrugation of about 0.4 nm, however, as they cover the entire Cu(1 1 1) surface their height with respect to the substrate cannot be determined. In either case their height is significantly larger than those of a mono-atomic step on the Cu(1 1 1) surface (0.21 nm) and the thickness of a Cu_2O(1 1 1) film (0.25 nm) [22], suggesting an involvement of more than a single copper layer and thus a Cu mass transport during their formation.

The charge exchange during the formation of the granular phase indicates an at least partial oxidation of the involved copper atoms. Even though the Pourbaix diagram [17] suggests the formation of a pure Cu(I)-oxide phase at about 200 mV more anodic potentials, attractive copper-phosphate interactions may facilitate the formation of a mixed copper-oxo-phosphate at lower potentials due to which we assign this phase to a mixed Cu(I)-oxo-phosphate species. However, it cannot be ruled out that also the deprotonation of involved (di)hydrogenphosphate anions contributes to the measured charge exchange. Once formed, this phase passivates the copper surface for the growth of thicker films until the onset of copper corrosion at potentials above +100 mV. Its stability is also reflected by the kinetic hindering of its reduction reaction, occurring at potentials close to the onset of HER, i.e. at about 300 mV more negative potentials with respect to its formation. Due to the overlap of the three reduction peaks, it is not possible to image the individual steps of the reduction reaction with STM, though a complete disappearance of the granular phase and a reappearance of the (4 × 4) phase can eventually be observed.

After few formation and decomposition cycles of the granular phase, the Cu(1 1 1) surface becomes significantly rougher and STM images show the formation of numerous additional islands (Fig. 4b). This implies a copper mass transport during the formation and decomposition of the granular phase and supports the previous assumption of a Cu mass transport during the formation of the granular phase. In contrast to e.g. Cl^- containing electrolytes [12], no healing up of these defects could be found at any potential, making STM imaging eventually impossible.

A possibility to prevent the roughening of the

Cu(1 1 1) surface is to limit the available Cu-amount, for example by depositing small amounts of copper on an inert substrate, e.g. Gold, a strategy which we will follow in the next sections.

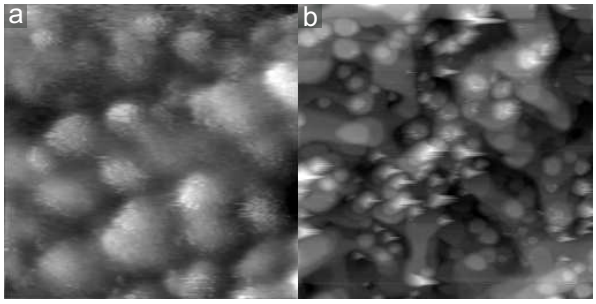

Figure 4: (a) Granular copper-oxo-phosphate phase, 14.5 × 14.5 nm^2, $E = -145$ mV, $U_B = 241$ mV, $I_T = 20$ nA; (b) roughening of surface after several oxidation/reduction cycles, 533 × 533 nm^2, $E = -445$ mV, $U_B = 108$ mV, $I_T = 20$ nA.

3.2. Au(1 1 1) in PO_4 Buffer Solution

Prior to the deposition of a Cu film, we characterize the behavior of the *Cu-free* Au(1 1 1) electrode in the same the phosphate buffer solution.

3.2.1. Cyclic voltammetry

A typical steady state CV curve for a Au(1 1 1) electrode in the phosphate buffer solution is shown in Fig 5. Its overall shape, which is dominated by a sharp anodic and a broad cathodic current peak at about 400 mV, is similar to that of Au(1 1 1) electrodes in more acidic 0.1 M H_3PO_3 solutions [23], however the CV curve for the more alkaline phosphate buffer solution, used in the present study, is shifted by about 200 mV to more negative potentials. Corresponding to previous FTIR studies [24], we assign the anodic peak to the adsorption and the cathodic peak to the desorption of phosphate anions, respectively. Considering the low degree of dissociation of an acidic phosphate solution, the shift of the phosphate adsorption in the present case to more negative potentials reflects the significantly different concentration of ionic $H_2PO_4^-$ and HPO_4^{2-} species in both electrolytes. In addition, the CV curve for the neutral phosphate buffer solution exhibits a second small peak pair at a potential of about +950 mV. Its appearance reminds of the well-known "butterfly" peak pair of many fcc(1 1 1) metals in sulfate containing electrolytes [1], in fact, CV curves for Au(1 1 1) in sulfate containing electrolytes exhibit a similar shape as those obtained for phosphate containing electrolytes [23]. Hence, it appears reasonable to interpret this peak pair in a similar fashion as being related with a phase transition of the adsorbed phosphate anions.

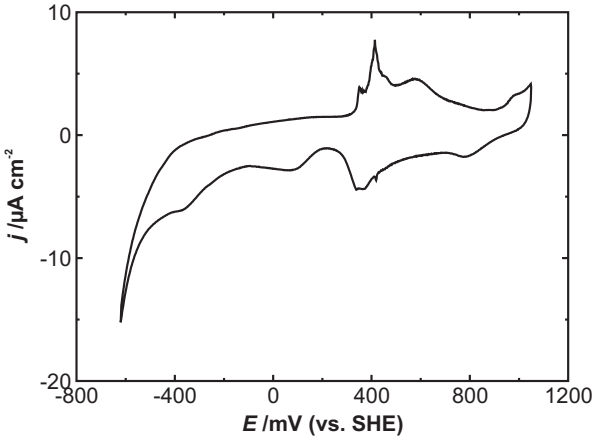

Figure 5: Cyclic voltammogram for a Au(1 1 1) electrode in a 0.05 M KH_2PO_4 + 0.05 M K_2HPO_4 solution, dE/dt = 10 mV s^{-}.

3.2.2. STM measurements

At potentials below 400 mV, i.e. more cathodic with respect to the sharp anodic current

peak in the CV curve, STM images show the typical double-stripe pattern of the Au(1 1 1) herringbone reconstruction (Fig. 6a), which propagates in the <2 1 1>-direction and appears, according to the substrate symmetry, in three rotational domains. Atomically resolved STM images (inset in Fig. 6a) clearly show the uniaxially compressed and apparently adsorbate free Au(1 1 1) surface.

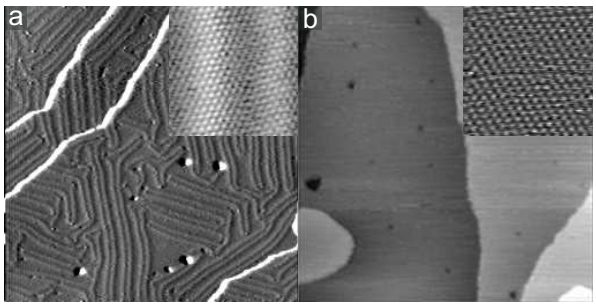

Figure 6: (a) Au(1 1 1) surface reconstruction at low potentials: 116 nm × 116 nm^2, $E = -538$ mV, $U_B = 4$ mV, $I_T = 10$ nA (differentiated for sake of visibility), **inset**: 4.77 × 4.77 nm^2, $E = -538$ mV, $U_B = 4$ mV, $I_T = 10$ nA; (b) Au(1 1 1)-(1×1) phase after lifting of the reconstruction: 112 × 112 nm^2, $E = 452$ mV, $U_B = 6$ mV, $I_T = 2$ nA, **inset**: 4.09 × 4.09 nm^2, $E = 425$ mV, $U_B = 50$ mV, $I_T = 10$ nA.

After increasing the potential to 450 mV, i.e. slightly positive from the sharp anodic peak in the CV curve, the herringbone reconstruction is lifted and instead the unreconstructed Au(1 1 1)-(1 × 1) phase is imaged (Fig. 6b). Beside the (1 × 1)-phase, no evidence of a phosphate adlayer, particularly regarding the results of our electrochemical and previous FTIR [24] characterizations, could be found under these conditions. A similar behavior is also known for Au(1 1 1) electrodes in sulfate containing electrolytes: after lifting of the surface reconstruction first a *mobile* sulfate adlayer is formed [1, 25], which cannot be imaged with STM. Hence also in the present case a mobile phosphate adlayer is formed after lifting of the Au(1 1 1) surface reconstruction.

In contrast to sulfate adlayers on Au(1 1 1) which undergo a complete phase transition to an immobile "($\sqrt{3} \times \sqrt{7}$)" phase [1, 25, 26], such transition could not be found for the present system. Even though the CV curve shows a similar feature (Fig. 5) as the so called "butterfly"-peak pair for the sulfate system, no complete phase transition was observed with STM under high-potential conditions. However, STM images recorded at such high potentials do show small patches with an at least partially ordered structure on fuzzy appearing terraces (Fig. 7). Despite their numerous defects, their structure can be described by parallel aligned close packed rows with a nearest neighbor distances of approx. 0.5 nm within a row and approx. 0.7 nm between adjacent rows, which are similar to those of the "($\sqrt{3} \times \sqrt{7}$)" structure of sulfate adlayers on Au(1 1 1) (0.499 nm and 0.762 nm, respectively).

The "($\sqrt{3} \times \sqrt{7}$)" sulfate adlayer structure is known to be stabilized by coadsorbed water species, such as hydronium or Zundel ions [1, 27], which form a zigzag-like structure in between adjacent close packed sulfate rows. The lower degree of order of the phosphate adlayer may indicate a lack of such an additional stabilization. Besides the stabilization of the structure, a coadsorbate may also screen the charge of the adsorbed anions and decrease thereby their repulsive coulomb interaction, which may have a strong effect in the present case due to the potentially higher charge of the adsorbed phosphate anions with respect to (bi)sulfate anions.

Both, shape and size of the patches change

rapidly, which indicates a continuous diffusion and hence a rather weak bonding of the adsorbed phosphate anions to the Au(1 1 1) substrate. During further potential increase, no further stabilization of the phosphate adlayer is observed, instead the substrate starts to oxidize at potentials of about +1100 mV and roughens significantly, in accordance with literature [28].

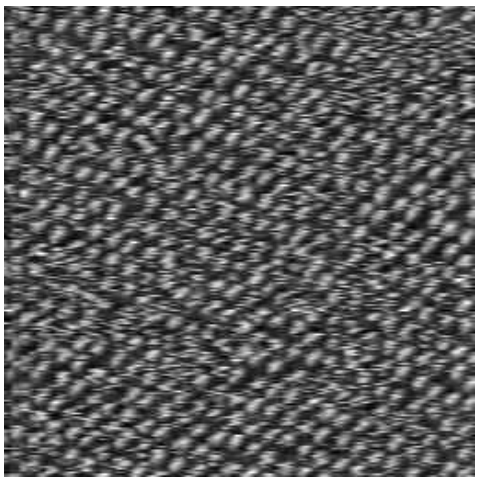

Figure 7: Patch of the partially ordered phosphate adlayer phase: 14.5 nm × 14.5 nm^2, E = 998 mV, U_B = 30 mV, I_T = 1 nA.

3.3. Cu modified Au(1 1 1) in PO_4 Buffer Solution

In the following, we report on the interaction of an ultrathin Cu-film on an Au(1 1 1) electrode with the phosphate buffer solution. Therefore, in a first step Cu is deposited on an Au(1 1 1) electrode and in a second step this Cu-modified electrode is exposed to the phosphate buffer solution.

3.3.1. Preparation of a Cu-submonolayer

Due to the low solubility of $Cu(OH)_2$ and $Cu_3(PO_4)_2$, the Cu-deposition on the Au(1 1 1) electrode cannot be carried out directly from the phosphate buffer solution. Instead a *sulfuric acid solution* is used for Cu-deposition, which is actually one of the best studied systems for metal underpotential deposition (upd), and allows the preparation of either a Cu-submonolayer with an exact coverage of a 2/3 monolayer or a full pseudomorphic Cu-monolayer on a Au(1 1 1) electrode [2, 29].

After deposition of a certain amount of copper, the remaining Cu^{2+} cations in the liquid phase have to be removed by a first electrolyte exchange for a *Cu-free sulfuric acid solution*. For this step, it is important to ensure that none of the deposited copper desorbs into the blank solution, which can be achieved by a controlled potential decrease of about 200 mV during the electrolyte exchange. Such an approach is already reported by Friebel et. al. [30, 31] for the preparation of ultrathin copper sulfide films on a Au(1 1 1) electrode. Our electrochemical and STM characterization of these first two preparation steps is in perfect agreement with these results.

After this first electrolyte exchange, the Au(1 1 1) surface is either covered with 2/3 ML of copper and 1/3 ML of coadsorbed sulfate anions or a full pseudomorphic Cu-monolayer. As both Cu-coverages exhibit a similar behavior in the phosphate buffer solution, the following discussion focuses mainly on the Cu-submonolayer, however, different behaviors of the full Cu-monolayer will be pointed out.

3.3.2. Transfer of the Cu-submonolayer into the phosphate buffer solution

After the first electrolyte exchange for a blank sulfuric acid solution, a second electrolyte exchange for the *phosphate buffer solution* was carried out.

Due to the pH change during this second electrolyte exchange from initial value of 1 in the sulfuric acid electrolyte to 6.8 in the phosphate buffer solution, the potential of the used Pt pseudo-reference electrode drops by 290 mV. As this electrolyte exchange is performed at a constant potential with respect to the pseudo-reference electrode, also the working electrode potential drops from typically 250 mV to about −50 mV.

Due to the geometry of the electrochemical cell, the working electrode will get in contact with the new electrolyte first and will be thereby subjected for a short time to the higher potential. However, the following will show that structure and morphology of the Cu-film are only affected at potentials above 400 mV. Hence the exposition to the higher potential at the beginning of the electrolyte exchange does not cause any uncontrolled changes to the Cu-film.

STM images recorded after the second electrolyte exchange exhibit significant morphological and structural changes of the Cu submonolayer with respect to the sulfuric acid electrolyte. Instead of being completely closed and homogeneous, it breaks up and vacancy islands are formed (upper right in Fig. 8a). Moreover, its morphology appears fuzzy and many domain borders can be found in STM images, which enclose 60° angles, according to the substrate symmetry (Fig. 8a). High resolution STM images of the Cu film exhibit a well ordered hexagonal structure with a nearest neighbor distance of (0.573 ± 0.006) nm and reveal the observed domain borders to be translational domain borders (Fig. 8b). Both, symmetry and nearest neighbor distance can be described with a (2×2) unit cell with an ideal lattice constant of 0.576 nm, which is further supported by the absence of any long-range modulation indicating a slight deviation from this commensurate to an alternative noncommensurate structure. As the Cu-free Au(1 1 1) surface appears adsorbate free under the same potential conditions, this structure can be clearly assigned to a coadsorbate phase of the Cu-submonolayer and an anion species.

For the structure of the 2/3 ML Cu-submonolayer in the initially used *sulfuric acid* electrolyte it is known, that 1/3 ML of coadsorbed sulfate anions forms a $(\sqrt{3} \times \sqrt{3})R30°$ structure by occupying the vacancies of an assumed pseudomorphic structure of the Cu-submonolayer [2, 29]. Assuming that also in the *present* system coadsorbed anions occupy vacancies, i.e. the defects of the Cu-submonolayer, implies a rearrangement of the Cu-submonolayer from its initial $(\sqrt{3} \times \sqrt{3})R30°$ in the *sulfuric acid* solution to a (2×2) defect structure in the *phosphate buffer* solution (Fig. 9). Due to the decreased defect density of the latter, 0.08 ML of vacancy islands must remain after the structural rearrangement of the Cu-submonolayer, which is in agreement with the vacancies found in STM images (Fig. 8a). The structural transition of the Cu-submonolayer is induced by the exchange of the initially coadsorbed sulfate anions by phosphate anions after the second electrolyte exchange.

The exchange of the coadsorbate and the corresponding structural transition of the Cu-submonolayer can also be directly imaged with STM: images recorded immediately after the electrolyte exchange for the phosphate buffer solution show a second phase with hexagonal symmetry in

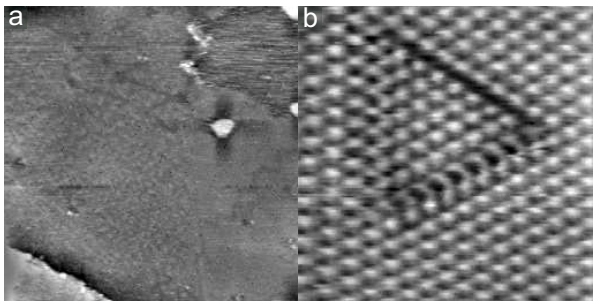

Figure 8: (a) Morphology, 113 × 113 nm^2, $E = -6$ mV, U_B = 101 mV, $I_T = 1$ nA; and (b) atomic structure of the Cu-submonolayer after electrolyte exchange for phosphate buffer solution, 9.33 × 9.33 nm^2, $E = -6$ mV, $U_B = 6$ mV, I_T = 2 nA.

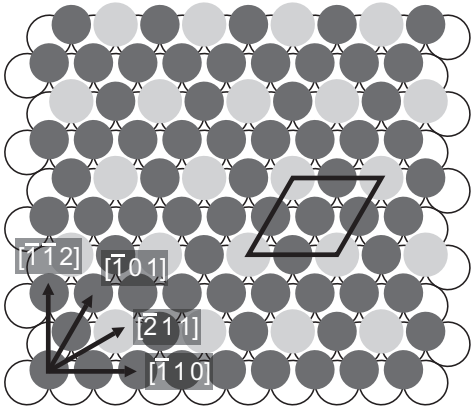

Figure 9: Model of the (2 × 2)–Cu–PO_4 coadsorbate phase (outlines circles: Au(1 1 1) substrate; dark gray: Cu, light gray: PO_4) with phosphate anions occupying the vacancies within the Cu-submonolayer.

the fuzzy appearing regions of the Cu-film (Fig. 10). Its lattice is rotated by 30° with respect to the (2 × 2) structure, i.e. it cannot be a symmetry equivalent, and has a lattice vector length of (0.501 ± 0.008) nm. Both fits perfectly to the $(\sqrt{3}\times\sqrt{3})R30°$ unit cell of the Cu–SO_4 coadsorbate structure of the Cu-submonolayer *before* it was exposed to the phosphate buffer solution. This structure disappears rapidly on favor of the (2×2) phase, which eventually covers the entire sample surface, except for the remaining 0.08 ML of vacancies.

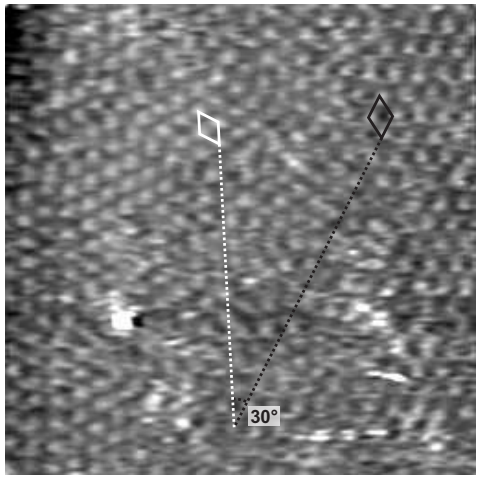

Figure 10: Coexisting (2 × 2)-Cu-PO_4 (black unit cell) and $(\sqrt{3}\times\sqrt{3})R30°$-Cu-$SO_4$ (white unit cell) coadsorbate structures, 9.53 × 9.53 nm^2, $E = -72$ mV, $U_B = 72$ mV, I_T = 10 nA.

The assumption that phosphate anions are coadsorbed in the vacancies of the Cu-submonolayer can be proved by exposing a *full* Cu-monolayer with a defect free pseudomorphic structure to the same electrolyte. Here, STM images recorded at the same potential at which the (2 × 2) structure was found for the Cu-submonolayer, show atomically smooth terraces without any evidence of the (2 × 2) coadsorbate phase (Fig. 11a). Only if the full Cu-monolayer is subjected to irreversible phase transitions at either very low or high potentials, the formation of domains of the (2 × 2)-Cu-PO_4 coadsorbate phase can be found (Fig. 11b). The nature of these potential induced phase transitions will be explained in detail in the following section.

Hence, after the electrolyte exchange for the phosphate buffer solution, the Cu-submonolayer has changed from its initial $(\sqrt{3}\times\sqrt{3})R30°$-Cu-$SO_4$ to a (2 × 2)-Cu-PO_4 coadsorbate phase, in which

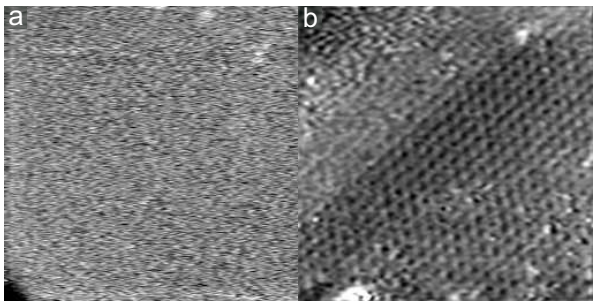

Figure 11: (a) Absence of phosphate adlayer on atomically terraces of the *full* Cu-monolayer, 14.1 × 14.1 nm^2, E = −115 mV, U_B = 14 mV, I_T = 1 nA; (b) appearance of (2 × 2) phase on the *full* Cu-monolayer after its exposure to low potentials, 12.0 × 12.0 nm^2, $E = -47$ mV, $U_B = 34$ mV, $I_T = 0.5$ nA.

coadsorbed phosphate anions occupy the vacancies of a (2 × 2) defect structure of a pseudomorphically arranged Cu-submonolayer on the Au(1 1 1) substrate.

3.3.3. Potential-induced phase changes

After deposition and transfer of the Cu-submonolayer into the phosphate buffer electrolyte, the sample potential was varied in both cathodic and anodic directions with 10 mV s^{-1}, starting each time with a freshly prepared sample at an initial potential of about −50 mV.

Decreasing the potential below −200 mV yields to a partial desorption of the coadsorbed phosphate anions and a transition of the Cu-submonolayer to a mobile 2-dimensional gas-like phase (Fig. 12a). Such a transition is already known for the Cu-submonolayer in sulfate containing electrolytes, where the CV curves show a distinctive cathodic peak which is correlated to the desorption of the coadsorbed sulfate anions, which stabilize its the honeycomb like structure [32]. In agreement with these results, the CV curves of the Cu-submonolayer in the *phosphate buffer* solution also show a sharp cathodic peak (curve #1 in Fig. 13) which can be correlated to the transition to the mobile phase in STM images. This order–disorder transition is reversible, upon subsequent potential increase an anodic peak is observed in the CV curves (curve #1 in Fig. 13) and STM images show the reappearance of the (2 × 2)-structure (Fig. 12b), which, however, has a significantly decreased average domain size with respect to the initially formed (2 × 2)–structure. In addition, this also proves the previous assumption that phosphate anions coadsorb in the (2 × 2) phase: alternatively coadsorbed sulfate species which might remain at the surface would have been infinitively diluted into the phosphate buffer electrolyte after their cathodic desorption. Both the change of the structure and the order-disorder transition of the Cu-submonolayer are another excellent example for the strong influence of coadsorbed anions on metal adlayers, similar as it is already known for small amounts of chloride [33].

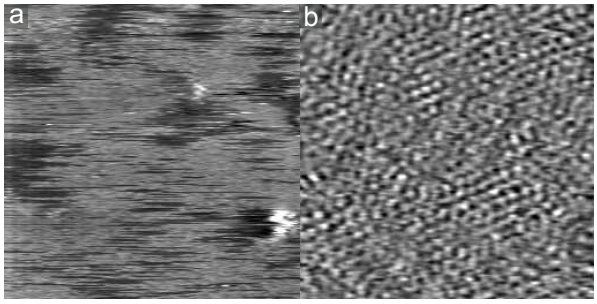

Figure 12: (a) Mobile Cu-adlayer after desorption of phosphate coadsorbate, 28.3 × 28.3 nm^2, $E = -245$ mV, U_B = 50 mV, I_T = 2 nA; (b) reappearance of (2 × 2) phase after phosphate adsorption, 12.8 × 12.8 nm^2, $E = -45$ mV, U_B = 8 mV, I_T = 20 nA.

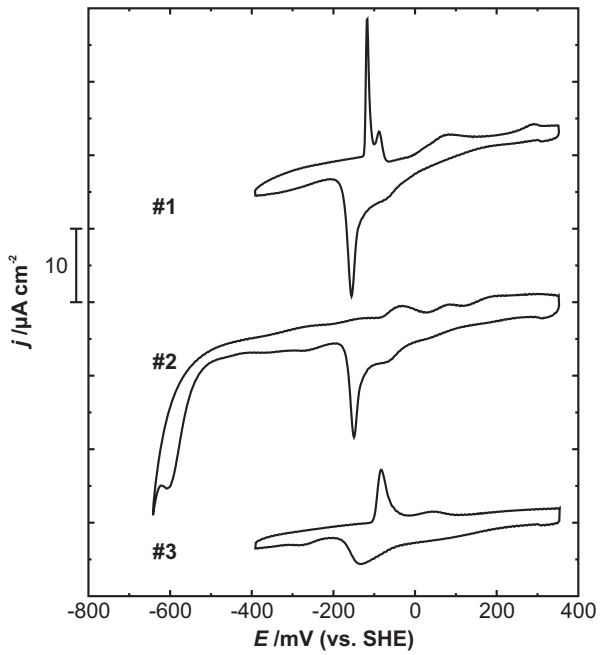

Figure 13: Series of CV curves for a Cu-covered Au(1 1 1) electrode in a 0.05 M KH_2PO_4 + 0.05 M K_2HPO_4 solution, dE/dt = 10 mV/s

However, if the potential range is extended in either anodic or cathodic direction over 400 mV or −500 mV, respectively, additional irreversible phase transitions can be observed.

After decreasing the potential below −500 mV, the mobile Cu-submonolayer becomes immobile again and coalescent islands are formed (Fig. 14a). Within the vacancies of the islands most likely the adsorbate free Au(1 1 1) surface is being imaged, however, it exhibits numerous small defects (arrow in Fig. 14a) and no evidence of the onset of the "Herringbone" reconstruction, as for the Cu-free system, can be found. The relative coverage of the islands can be estimated to about 2/3 ML, consistent with the initial Cu-coverage. However their low height of 0.11 nm with respect to the vacancies is only about half of what would be expected from a geometric hard sphere model of Cu-atoms occupying 3-fold hollow-sites on a Au(1 1 1) surface (0.235 nm). In addition they appear rather inhomogeneous and exhibit surprisingly an amorphous but not pseudomorphic structure in high-resolution STM images (Fig. 14b).

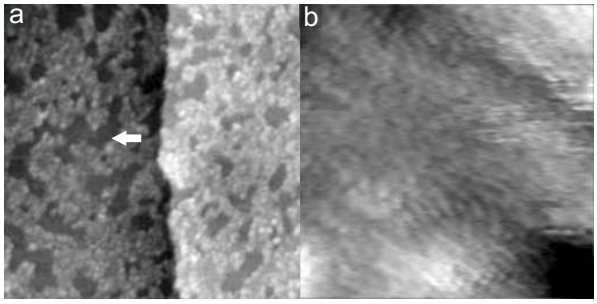

Figure 14: (a) Immobile Cu-adlayer at low potentials, 106 × 106 nm^2, E = −555 mV, U_B = 100 mV, I_T = 10 nA; (b) amorphous structure of immobile Cu-phase, 5.37 × 5.37 nm^2, E = −548 mV, U_B = 4 mV, I_T = 30 nA.

Corresponding to the phase transition in STM images, the CV curve shows a cathodic shoulder close to the onset of the HER (curve #2 in Fig. 13) and during the back-scan in anodic direction the sharp peak, which corresponds to the adsorption of phosphate anions on the Cu-submonolayer, is suppressed. However, it reappears slowly during several potential cycles after limiting the scan range in cathodic direction to −400 mV again (curve #3 in Fig. 13; 7th potential cycle in limited scan range after curve #2), but remains even after many cycles significantly broader and weaker as in the initial potential scan. Subsequent recorded STM images show at the same potential at which the initial (2 × 2)-Cu–PO_4 coadsorbate phase was found, a rather defective surface with some granular particles and only small domains of the (2 × 2) structure

(Fig. 15a). Hence, both electrochemical and STM measurements indicate that the Cu-submonolayer has become partially inert for the formation of the Cu–PO_4 coadsorbate phase after being exposed to low potentials, i.e. after its transition to the immobile phase.

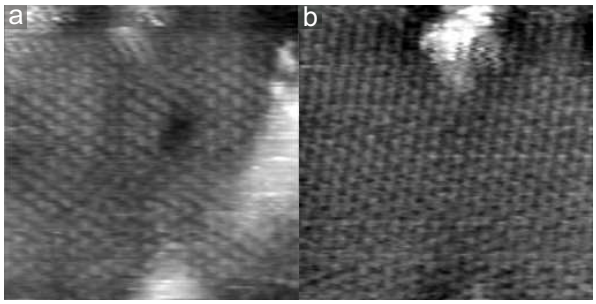

Figure 15: Reappearance of (the 2×2) phase either after (a) anodic phosphate readsorption on immobile Cu-adlayer, 10.7×10.7 nm^2, $E = -7$ mV, $U_B = 52$ mV, $I_T = 10$ nA; or (b) reduction of the amorphous oxidized copper film, 11.5×11.5 nm^2, $E = 255$ mV, $U_B = 37$ mV, $I_T = 20$ nA.

In general, the transition from the mobile to the immobile phase can be attributed to an increased bonding strength of the Cu-submonolayer to the Au(1 1 1) substrate. The corresponding peak in the CV curve indicates a charge exchange of the Cu-submonolayer with the substrate during this phase transition. Both effects can be explained by a *two-step* desorption mechanism of the coadsorbed phosphate anions: Starting with the initial (2×2)-Cu–PO_4 coadsorbate phase, only some of the phosphate anions are desorbed during the *first* phase transition of the Cu-submonolayer to the mobile phase, whereas the remaining phosphate anions are desorbed during the *second* phase transition to the immobile phase.

Hence, also the mobile phase must be interpreted as a Cu–PO_4 coadsorbate phase, but with a decreased PO_4 coverage with respect to the immobile (2×2)-Cu-PO_4 coadsorbate phase. The remaining attractive Cu–PO_4 interactions reduce the bonding strength of the Cu-submonolayer to the substrate, which causes its high mobility. Due to the fast desorption of the residual phosphate anions during the phase transition to the immobile phase, these attractive Cu–PO_4 interactions disappear abruptly, yielding in a sudden condensation of the Cu-submonolayer. Its resulting amorphous structure is stabilized by the slow diffusion of the Cu-atoms due to their strong binding to the Au(1 1 1) surface.

The irreversible character of this phase transition stems from a hindering of the phosphate adsorption on the amorphous Cu-film, most likely it does not provide suitable adsorption sites, similar to the full Cu-monolayer. Only at its step edges a restructuring appears reasonably easy which eventually provides suitable adsorption sites, causing the weak phosphate ad/desorption peak in the CV curves and the small domains of the (2×2) structure in STM images (Fig. 15a).

However, the small defects on the Au(1 1 1) terraces may also suggest an incorporation of Au-atoms, supplied by the substrate, into the islands of the amorphous phase and thereby an alternative interpretation as a Cu–Au alloy phase rather than a pure Cu-film. In either case, the low height of the islands with respect to the surrounding Au(1 1 1) surface does not reflect its topological height but is probably caused by a reduced density of states on the islands, yielding in a lowered appearance in STM. An alternative interpretation of their low height as being caused by an inversion of the verti-

cal stacking, i.e. an Au termination of the islands and a diffusion of Cu into the second layer as observed on Au_3Cu surfaces [34], appears unlikely due to the absence of large scale defects of the Au(1 1 1) substrate in STM images and the fast transition from the mobile to the amorphous phase. The particles observed after subsequent potential increase (Fig. 15a) are most likely coalescent, bulk-like Cu-particles that appear inert for phosphate adsorption due to the lack of suitable adsorption sites. Both the interesting structural properties and the chemical identity of the immobile phase call for further studies using different techniques.

Increasing the potential after preparation of the (2×2) phase to above +400 mV results in an oxidation of the Cu-submonolayer. The corresponding CV curve (Fig. 16) shows for both, oxidation and subsequent reduction of the Cu-submonolayer, only a single distinguished peak pair at about 400 mV. The charge exchange for both processes corresponds to about 2 electrons per copper atom, indicating a direct Cu(0)–Cu(II) transition. The stabilization against the oxidation towards an intermediate Cu(I) phase, as it is suggested by the Pourbaix diagram, is also reported for Cu covered Pt clusters [35] and is denoted to attractive interactions of the deposited copper with its support. In addition, they also stabilize the Cu-submonolayer in the present system for its dissolution into the Cu-free phosphate buffer solution, whereas for the bulk Cu(1 1 1) electrode the onset of Cu corrosion was observed at a potential of +100 mV. By comparison with the *Cu-free* Au(1 1 1) electrode (Fig. 5) is becomes clear that the oxidation of the Cu-submonolayer and the lifting of the "herringbone" reconstruction occurs at the same potential, i.e. +400 mV. Hence the gain in surface free energy by the onset of surface reconstruction for the Cu-free system, stabilizes the Cu-submonolayer for dissolution on the unreconstructed Au(1 1 1) surface.

STM images of the oxidized Cu-submonolayer show a closed-film like morphology with several additional small particles (Fig. 17a), but no atomic order can be found in high-resolution STM images (Fig. 17b). The closed morphology and the appearance of additional particles indicate a significant lateral expansion of the Cu-submonolayer during its oxidation, yielding in a structure which is determined by Cu–O interactions rather than by interactions with the Au(1 1 1) substrate. After reduction, the (2×2) phase reappears in STM images (Fig. 15b), though the small particles, which have been formed during the oxidation of the Cu-submonolayer, can still be detected. The oxidized phase might be either a bulky CuO or a $Cu_3(PO_4)_2$ like phase, however, considering the behavior of the bulk Cu(1 1 1) electrode in the same electrolyte it appears reasonable to assign at least the additional particles to a copper-oxo-phosphate like species.

4. Discussion and Summary

We have studied the interaction of Cu(1 1 1), Au(1 1 1) and Cu-covered Au(1 1 1) electrodes with a neutral phosphate buffer electrolyte and found the formation of ordered phosphate anion adlayers on all three surfaces:

- a partial $(\sqrt{3} \times \sqrt{3})R30°$-$PO_4$ phase for Cu(1 1 1) (nominal $\Theta = 0.33$ ML),

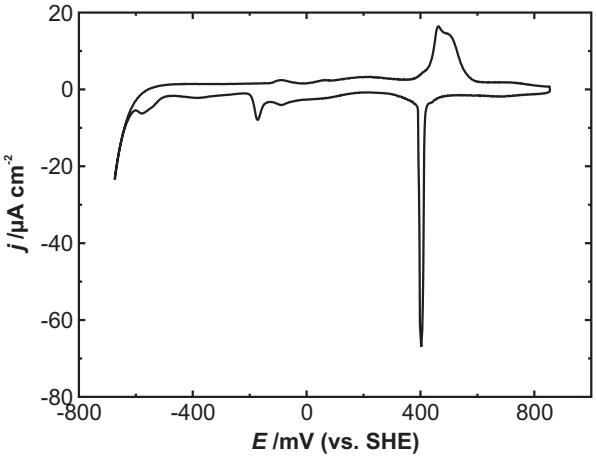

Figure 16: CV curve for the oxidation/reduction of a Cu-submonolayer on Au(1 1 1) in a 0.05 M KH_2PO_4 + 0.05 M K_2HPO_4 solution, dE/dt = 10 mV s^{-1}

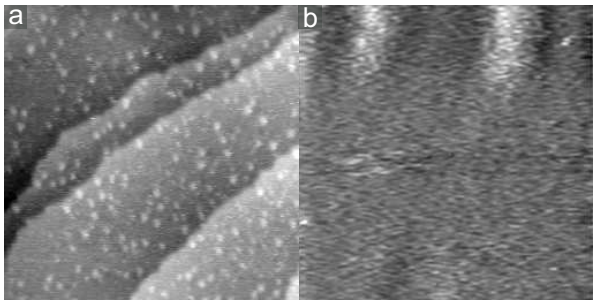

Figure 17: (a) Morphology, 113 × 113 nm^2, E = 760 mV, U_B = 50 mV, I_T = 10 nA; and (b) amorphous structure of the oxidized Cu-submonolayer, 14.1 × 14.1 nm^2, E = 760 mV, U_B = 50 mV, I_T = 10 nA.

- a partial "$(\sqrt{3} \times \sqrt{7})$"-$PO_4$ phase for Au(1 1 1) (nominal Θ = 0.20 ML) and
- a (2 × 2)-Cu-PO_4 coadsorbate phase for a Cu-submonolayer on Au(1 1 1) (nominal Θ = 0.25 ML).

By comparing these systems, it becomes obvious that the nominal phosphate coverage increases in the order of Au(1 1 1) < Au(1 1 1)-Cu < Cu(1 1 1), thus with increasing Cu-amount at the electrode surface. The higher affinity of phosphate anions to copper than to gold results from their bonding with oxygen atoms to the surface and is hence predicted by the oxygen affinity of the substrate, which is naturally higher for copper than for gold.

However, only on the Cu-submonolayer covered Au(1 1 1) surface the phosphate adsorbate layer covers the entire surface, except for 0.08 ML of vacancies due to the low initial Cu-coverage, whereas on the bulk Cu(1 1 1) and Au(1 1 1) electrodes just few adlayer patches are formed, and most of the adsorbed phosphate anions remain in a mobile 2-dimensional gas-like phase. In contrast to the bulk Cu(1 1 1) and Au(1 1 1) electrodes, the Cu-submonolayer on the Au(1 1 1) electrode undergoes a lateral rearrangement during phosphate adsorption due to which phosphate anions are adsorbed in a (2 × 2) defect structure of the Cu-submonolayer which has a significantly higher corrugation than the bulk electrode surfaces and thus stabilizes the phosphate adlayer. In comparison to sulfate, which is known to form closed adlayers on Cu(1 1 1) and Au(1 1 1) surfaces, the potentially higher charge and thereby stronger Coulomb repulsion of the adsorbed phosphate anions may inhibit the formation of closed adlayers.

At low potentials, which are of interest for the envisioned electrochemical CO_2 reduction, both the Au(1 1 1) and the Cu(1 1 1) surface appear apparently adsorbate free, indicated by the presence of the "herringbone" reconstruction and the formation of a characteristic (4×4) phase, respectively. In the case of Cu(1 1 1), however, the morphology of the electrode is heavily influenced by the formation of a copper-oxo-phosphate phase at intermediate potentials and roughens significantly after few phosphate

adsorption/desorption cycles.

For the Cu-covered Au(1 1 1) electrode, a phase transition from a 2-dimensional gas-like to an immobile phase was found during potential decrease after phosphate desorption. Surprisingly, the immobile Cu-adlayer phase exhibits an amorphous structure and some evidence is found that it might even be an Au–Cu-alloy phase. In either case it does not stay in a pseudomorphic structure, moreover its amorphous structure may exhibit interesting properties, e.g. in its catalytic behavior, and will be subject to further investigation.

5. Acknowledgments

The Center for Individual Nanoparticle Functionality (CINF) is sponsored by The Danish National Research Foundation.

[1] O.M. Magnussen, Chem. Rev. 102 (2002) 679.

[2] E. Herrero, L.J. Buller, H.D. Abruña, Chem. Rev. 101 (2001) 1897.

[3] C. Graves, S.D. Ebbesen, M. Mogensen, K.S. Lackner, Renewable Sustainable Energy Rev. 15 (2011) 1.

[4] Y. Hori, H. Wakebe, T. Tsukamoto, O. Koga, Electrochim. Acta 11/12 (1994) 1833.

[5] M. Gattrell, N. Gupta, A. Co, J. Electroanal. Chem. 594 (2006) 1.

[6] Y. Hori, in: C. Vayenas et al. (Eds.), Modern Aspects of Electrochemistry, Number 42, Springer, New York, 2008, pp. 89-189.

[7] A.A. Peterson, F. Abild-Pedersen, J. Rossmeisl, J.K. Nørskov, Energy Environ. Sci. 3 (2010) 1311.

[8] A.A. Peterson, J.K. Nørskov, J. Phys. Chem. Lett. 3 (2012) 251.

[9] P. Strasser, S. Koh, T. Anniyev, J. Greeley, K. More, C. Yu, Z. Liu, S. Kaya, D. Nordlund, H. Ogasawara, M.F. Toney, A. Nilsson, Nat. Chem. 2 (2010) 454.

[10] K.J.P. Schouten, Z. Qin, P. Gallent, M.T.M. Koper, J. Am. Chem. Soc. 134 (2012) 9864.

[11] M. Wilms, M. Kruft, G. Bermes, K. Wandelt, Rev. Sci. Inst. 70 (1999) 3641.

[12] P. Broekmann, M. Wilms, M. Kruft, K. Wandelt, J. Electroanal. Chem. 467 (1999) 307.

[13] G. Niaura, A.K. Gaigalas, V.L. Vilker, J. Phys. Chem. B 101 (1997) 9250.

[14] V. Maurice, L.H. Klein, H.H Strehblow, P. Marcus, J. Electrochem. Soc. 150 (2003) B316.

[15] D. Friebel, P. Broekmann, K. Wandelt, Phys. Stat. Sol. A 201 (2004) 861.

[16] Y.S. Chu, I.K. Robinson, and A.A. Gewirth, J. Chem. Phys. 110 (199) 5952.

[17] M. Poubaix, Atlas of Electrochemical Equilibria in Aqueous Solutions, first ed., Pergamon, Oxford, 1966.

[18] P. Broekmann, M. Wilms, K. Wandelt, Surf. Rev. Lett. 6 (1999) 907.

[19] D. Friebel, T. Mangen, B. Obliers, C. Schlaup, P. Broekmann, K. Wandelt, Langmuir 20 (2004) 2803.

[20] H. Matsushima, A. Taranovskyy, C. Haak, Y. Gründer, O.M. Magnussen, J. Am. Chem. Soc. 131 (2009) 10362.

[21] H. Matsushima, C. Haak, A. Taranovskyy, Y. Gründer, O.M. Magnussen, Phys. Chem. Chem. Phys. 12 (2010) 13992.

[22] J. Kunze, V. Maurice, L.H. Klein, H.H. Strehblow, P. Marcus, J. Phys. Chem. B 105 (2001) 4263.

[23] A. Cuesta, M. Kleinert and D.M. Kolb, Phys. Chem. Chem. Phys. 2 (2000) 5684.

[24] M. Weber, F.C. Nart, Electrochim. Acta 41 (1996) 653.

[25] K. Suto, O.M. Magnussen, J. Electroanal. Chem. 649 (2010) 136.

[26] O.M Magnussen, J. Hageböck, J. Hotlos, R.J. Behm, Faraday Discuss. 94 (1992) 329.

[27] T. Wandlowski, K. Ataka, D. Diesing, Electrochim. Acta 49 (2004) 1233.

[28] M.A. Schneeweiss, D.M. Kolb, Solid State Ionics 94 (1997) 171.

[29] M. Nakamura, O. Endo, T. Ohta, M. Ito, Y. Yoda, Surf. Sci 514 (2002) 227.

[30] D. Friebel, C. Schlaup, P. Broekmann, K. Wandelt, Surf. Sci 600 (2006) 2800.

[31] D. Friebel, C. Schlaup, P. Broekmann, K. Wandelt, Phys. Chem. Chem. Phys. 9 (2007) 2142.

[32] C.E. Täubert, M. Petri, D.M. Kolb, Z. Phys. Chem.

221 (2007) 1493.

[33] J. Hotlos, O.M. Magnussen, R.J. Behm, Surf. Sci 335 (1995) 129.

[34] G.A. Eckstein, S. Maupai, A.S. Dakkouri, M. Stratmann, M. Nielsen, M.M. Nielsen, R. Feidenhans'l, J.H. Zeysing, O. Bunk, R.L. Johnson, Phys. Rev. B60 (1999) 8321.

[35] P. Borthen, B.J. Hwang, H.H. Strehblow, D.M. Kolb, J. Phys. Chem. B 104 (2000) 5078.